Iranian Journal of Geophysics, 2017, Page 1 - 9

The transition energy and the beaming angle of converted LO-mode waves from 100 to 400 kHz through density gradient according to observations of kilometric continuum radiations in the plasmapause

Mohammad Javad Kalaee [1*] and Yuto Katoh [2]

[1] *Assistant Professor, Institute of Geophysics, University of Tehran, Tehran, Iran*
[2] *Department of Geophysics, Graduate School of Science, Tohoku University, Sendai, Japan*

(Received: 09 April 2016, Accepted: 06 August 2016)

Abstract

The satellite observations such as the Cluster mission with four-point measurements show some local fluctuations in the density gradient in the vicinity of the plasmapause. These structures are found over a broad range of spatial scales, with a size from 20 to 5000 km. Also, the simultaneous observations of the kilometric continuum by IMAGE (Imager for Magnetopause-to-Aurora Global Exploration) and GEOTAIL satellites have indicated another new evidence of a very broad emission. In this study, we considered the mode conversion of waves propagating under the presence of the density gradient in a scale length from 20 to 10,000 km, for a range of frequency from 100 to 400 kHz according to observations of the kilometric continuum. We calculated the transmitted energy flux as a function of the spatial scale lengths and the frequencies. We also calculated the resultant beaming angle for the frequency and the wave normal angle of incident waves. For these cases, results showed that the beaming angle becomes larger and smaller than the angle estimated by Jones' formula. We suggest that the spatial scale length should be less than about 100 km for the efficient mode conversion and then that the beaming angle becomes consistent with the observed the kilometric continuum.

Keywords: beaming angle, scale length, Cluster mission, kilometric continuum

[*]Corresponding author: mjkalaee@ut.ac.ir

1 Introduction

The mode conversion, identified as a change of propagation modes of plasma waves (Stix, 1992), is one of the generation mechanisms of radio emissions occurring in an inhomogeneous plasma. The mode conversion from Z-mode (extraordinary) wave to LO-mode (ordinary) wave has been investigated for the purpose of understanding the origin of planetary radio emissions (Warren and Hagg, 1968; Oya, 1971, 1974; Jones, 1980, 1981).

Jones et al. (1987) and Jones (1988) applied the LMCW (linear mode conversion "window") theory to explain the generation process of nonthermal continuum radiation. The term "window" for radio waves in a stratified magneto plasma is used to denote the phenomenon whereby waves in one magneto-ionic mode can penetrate through an evanescent region, according to a simple ray theory, and turn into a different magneto-ionic mode on the far side (Eliss, 1956; Budden, 1980, 1985). The prediction of LMCW is that the LO-mode radiation emanating from the radio window is beamed away from the magnetic equatorial plane at an angle given as follows (Jones, 1988):

$$\alpha_{LMCT} = \tan^{-1}\left(\frac{\omega_c}{\omega_p}\right)^{1/2}, \qquad (1)$$

where, ω_c, ω_p and α_{LMCT} represent the electron cyclotron frequency, plasma frequency and the beaming angle from LMCT (linear mode conversion theory) prediction, respectively. This relation works only for a free propagating wave in a weakly inhomogeneous medium. The frequency of waves emitted from the radio window is determined by the local plasma frequency at the site of mode conversion. In general, we defined α as the beaming angle with respect to the magnetic equatorial plane.

Recent satellite observations have indicated the beaming angle theory (Jones, 1980; Jones et al., 1987) is not always consistent with these observations (Hashimoto et al., 2006; Boardsen et al., 2008). On the other hand, recent satellite observations, such as the Cluster mission with four-point measurements have made it possible to study the geometry of these density structures. These structures are found over a broad range of spatial scales with a minimum size of about 20 km (Darrouzet et al., 2004, 2006).

Previous studies showed that for a p value of the incident angle (the so-called critical wave normal angle of the incident wave), an extraordinary (Z-) mode wave, propagating toward an inhomogeneous plasma slab, may be converted to ordinary (LO) mode waves with a maximum rate (Jones, 1980, 1981; Kalaee et al., 2009, 2010). According to the cold plasma theory, for another value of the wave normal angle of the incident wave, the mode conversion efficiency is strongly reduced, since a region of evanescence develops between two branches of extraordinary and ordinary mode waves. The geometrical size of this evanescent region depends on the density scale length (L), and a considerable fraction of the energy flux can be transmitted through this region, if L becomes small (Mjulhus, 1984; Kalaee and Katoh, 2014a).

In this study, we considered a scale length from 20 to 10,000 km, and a range of frequencies from 100 to 400 kHz according to observations of the kilometric continuum (Hashimoto et al., 2006). We calculated the transmitted energy flux via the spatial scale lengths and the frequencies. We calculated the beaming angle via the frequency. We showed the beaming angle became different from the Jones' formula given by (1).

2 Model and calculation

Based on the cold plasma theory, for the conversion of the extraordinary to ordinary mode waves to be possible, the parallel component of the refractive index of the incident waves, $n_{\|}$, should be equal to

$$n_{\|}^2 = (n_{\|}^c)^2 = \frac{Y}{1+Y}, \quad (2)$$

where $n_{\|}^c$ is a critical value for the parallel component of the refractive index, and $Y = \omega_c/\omega$, where ω is the frequency of the incident wave. By considering the dispersion relation for waves in cold plasma, we obtain

$$n^2 = n_{\|}^2 + n_{\perp}^2 = 1 - \frac{2X(X-1)}{2(X-1) - Y^2\sin^2\theta \pm \Gamma}, \quad (3)$$

where n is the refractive index, $n_{\|}$ and $n_{\perp}$ are the parallel and perpendicular components of the refractive index (as referred to the magnetic field), respectively,

$$\Gamma = \left[Y^4\sin^4\theta + 4(X-1)^2 - Y^2\cos^2\theta\right]^{1/2}, \quad (4)$$

where, $X = (\frac{\omega_p}{\omega})^2$, $Y = \frac{\omega_c}{\omega}$, θ is the wave normal angle, and the + (-) sign gives the refractive index of the Z- (LO-) mode. It is clear from equation (3) that the two modes coalesce when the quantity Γ vanishes, and the equation (2) is obtained.

Therefore, for a certain value of the incident angle the quantity Γ vanishes, and the two modes are matched. Figure 1 shows the variation of the wave normal angle θ with the local plasma frequency ω_p/ω_c for the case of $\omega = 2.03\omega_c$. The solid green curve shows an example of the matching case, so that equation (2) is satisfied (for example in a layer with $\omega_p/\omega_c = 2$, the incident wave normal angle should be 58.3°).

When $(n_{\|})^2 \neq (n_{\|}^c)^2$, the two branches of extraordinary and ordinary waves are mismatched and there is a region of evanescence between the two branches. The dash-dotted red curve in Figure 1 shows an example of this case. The parameters are the same as those used in the green curve, but the incident wave normal angle is different (for example in a layer with $\omega_p/\omega_c = 2$, the incident wave normal angle is equal to 64°).

The transmitted energy flux via the spatial scale lengths is calculated based on the cold plasma theory (Mjulhus, 1984):

$$T(n_{\perp}+n_{\|}) = \exp\left\{-\pi k_0 L\sqrt{\frac{Y}{2}\left[2(1+Y)(n_{\|}^c - n_{\|})^2 + n_{\perp}^2\right]}\right\}, \quad (5)$$

where, $T(n_{\perp}+n_{\|})$ is the power transmission function, k_0 is the wavenumber of the ordinary wave in the vacuum, and L is the density scale length.

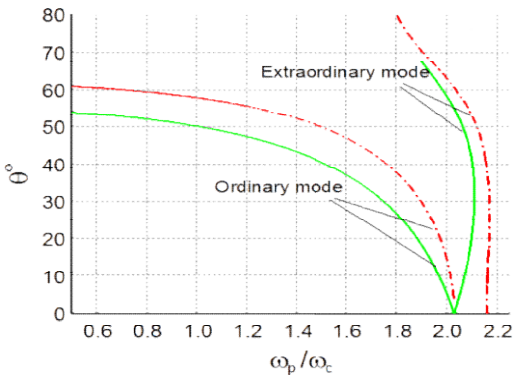

Figure 1. Variation of the wave normal angle θ with the local plasma frequency ω_p/ω_c for the case that $\omega = 2.03\omega_c$. For the solid green curve, the two modes are matched, ($n_{\|} = n_{\|}^c$), but for the dash-dotted red curve, the two mode waves are mismatched, ($n_{\|} \neq n_{\|}^c$). For this case, a region of evanescence develops between the two branches.

We calculated the power of energy transmission for a large range of spatial scale lengths from 20 to 10,000 km and a frequency range of the kilometric radiation from 100 to 400 kHz (Hashimoto et al., 2006). Next, we presented the results of beaming angle based on the numerical solution for each case.

3 Results and discussion

Figures 2a to 2f show the results of the power transmission function via variation of the wave normal angles around the critical angle (including the critical wave normal angle) for different values of the spatial scale length (L) and different frequencies. It is clear from Figure 2 that for $\theta = \theta_{\text{critical}}$, the transition energy is independent of the spatial scale length, and T has a maximum value at the critical angle. But, for $\theta \neq \theta_{\text{critical}}$ (there is an evanescent region, see Figure 1), the transition energy strongly depends on L, and just for a limited range of the wave normal angle variation around the critical angle, there is a significant transition energy; with decreasing L, this range becomes larger. Also, Figure 2 shows that with increase in the frequency, this limitation increases and there is a narrow range of the wave normal angle variation for the significant transition energy. For example, for L = 20 km, this range of the wave normal angle can reach $\pm 8^{\circ}$ (with T $\approx$ 0.2) for a frequency of 100 kHz as shown in Figure 2a, and this range is about $\pm 4^{\circ}$ for a frequency of 400 kHz as shown in Figure 2f. So, if there is an evanescent region, only for a limited range of the L, we expect that the mode conversion to occur and that the energy is transmitted. If such event occurs, then the beaming angle is not consistent with the conventional LMCT.

We calculated the beaming angles according to the initial parameters given in Table 1. We can obtain the beaming angle α with respect to the magnetic equatorial plane by $\alpha = 90 - \theta$, where θ is the wave normal angle of the LO-mode waves in free space. Figures 3a to 3f show the results of the power transmission function via the beaming angle for different values of spatial scale length (L) and different frequencies. The results show that with decrease in L, the variation of beaming angle increases and the beaming angle can become different from the LMCT prediction. Also it can be seen from Figure 3 that the range of this variation decreases as the frequency increases. The peaks of the curves are related to the matching cases ($\theta = \theta_{\text{critical}}$). To better understand this object, we calculated the beaming angles via a variation of the incident wave normal angles around the critical angle for different frequencies. As shown in Figure 4, where $\theta = \theta_{\text{critical}}$, the beaming angle is consistent with the conventional LMCT. But for $\theta \neq \theta_{\text{critical}}$, the beaming angle can be larger or smaller than the estimated angle by the Jones' formula (equation (2)). The CRRES (Combined Release and Radiation Effects Satellite) and IMAGE (Imager for Magnetopause-to-Aurora Global Exploration) satellites observed the kilometric continuum in wide latitudes including the equator, which such observations are not consistent with the beaming theory (Hashimoto et al., 2006). In Figure 4, the black circles show the beaming angles observed with multiple satellites with the source at 3.9 Re (Hashimoto et al., 2006), where Re is the radius of the Earth. The observed beaming angles are different from those predicted by the theory (values with $\theta = \theta_{\text{critical}}$). Therefore, under the condition that efficient mode conversion is

expected due to the effect of the steep density gradient (small L), the radio window angle of ordinary mode waves could be different from the LMCT prediction, as recently pointed out by the observational results. For these cases, the size of L determines the efficiency of mode conversion.

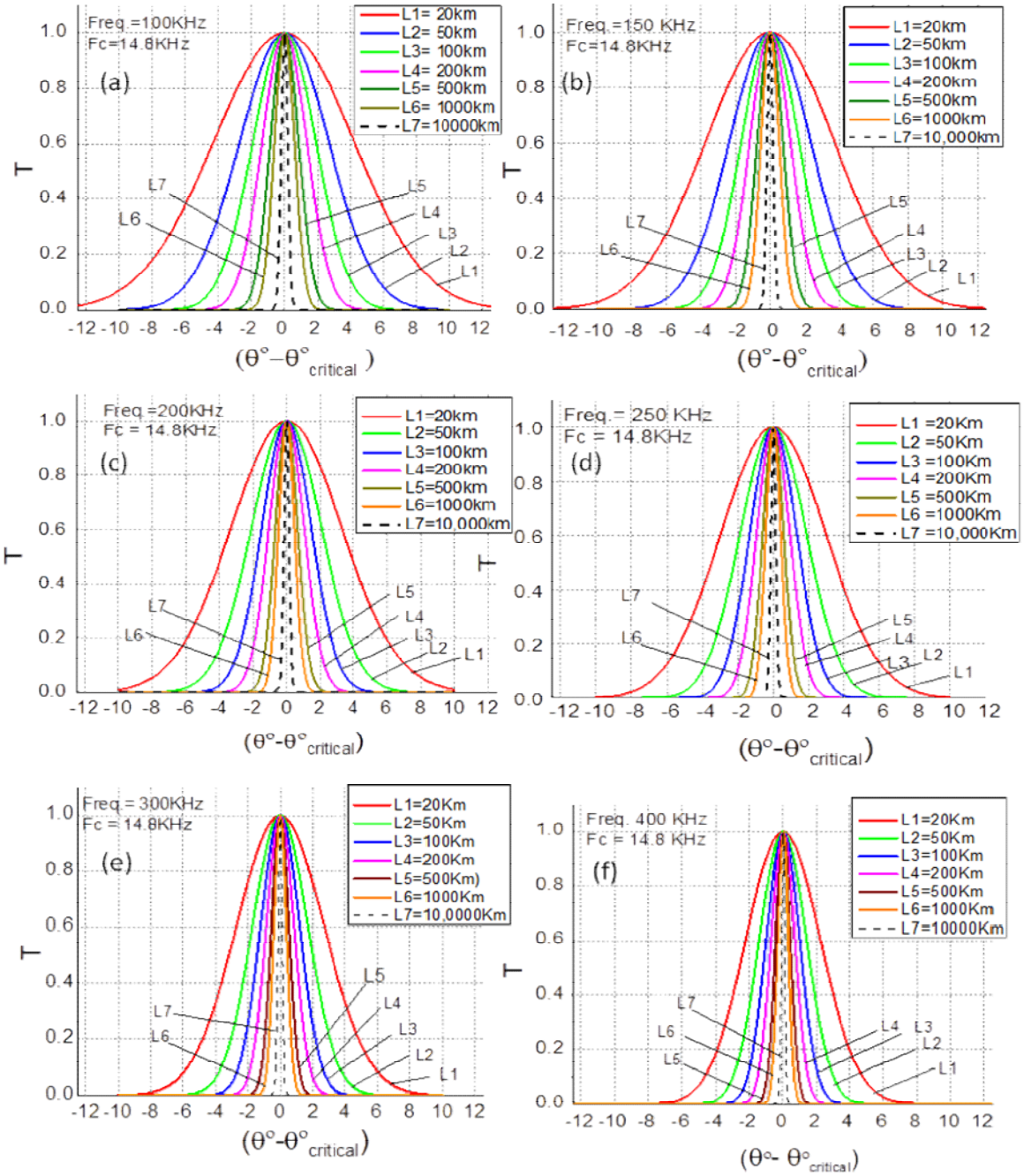

Figure 2. The power transmission function variation with the wave normal angles around the critical angle (including the critical wave normal angle) for different values of the spatial scale lengths (L) and different frequencies. It can be seen from (a) to (f) that the transition energy is significant for a limited range of the wave normal angle variation around the critical angle. Further, with the increase in the frequency, this limitation becomes ever more important.

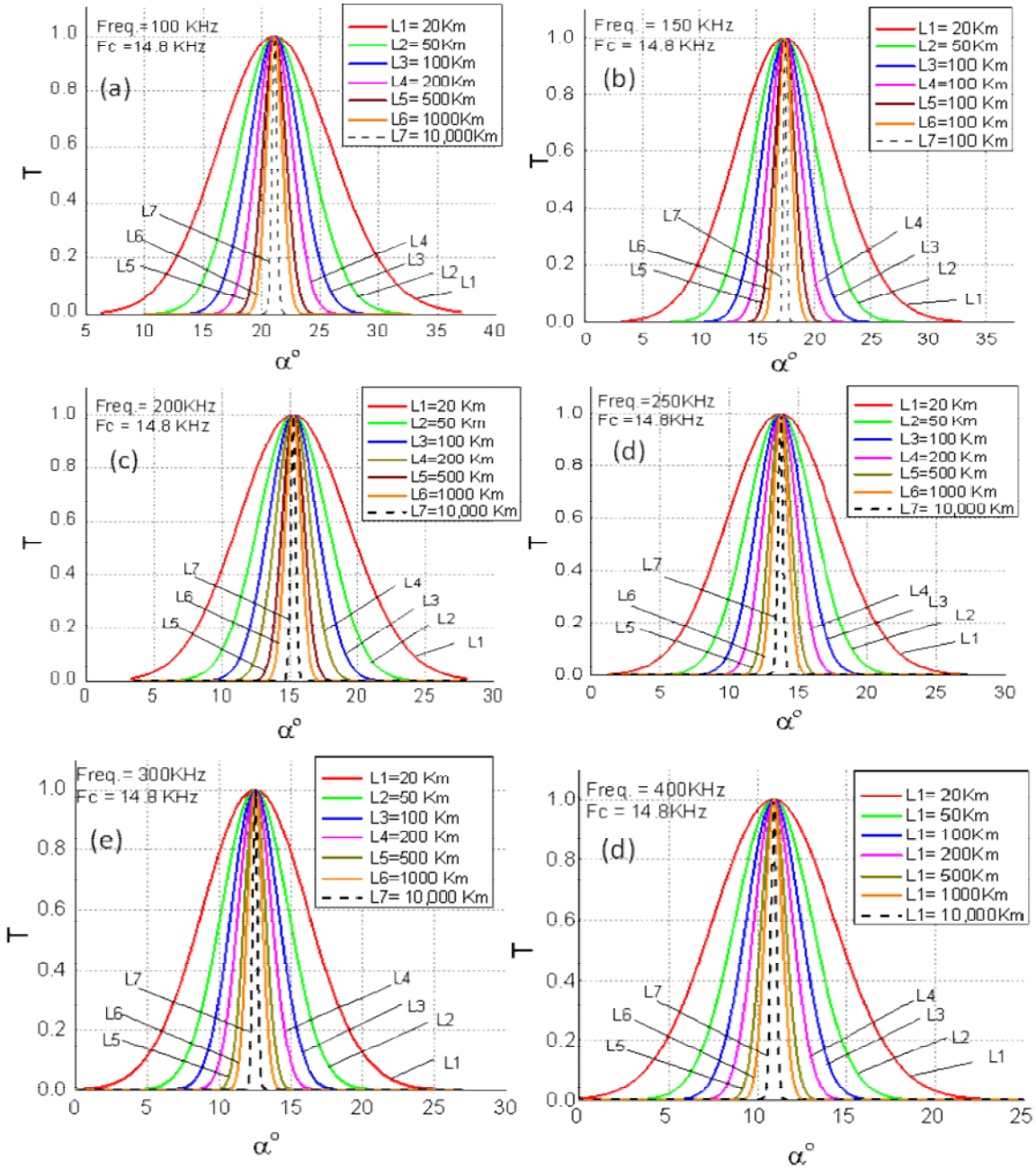

Figure 3. The power transmission function variation with the beaming angle (α) for different values of the spatial scale length (L) and different frequencies. The results show that with a decrease in L, the variation of beaming angle increases and the beaming angle can become different from the LMCT prediction. Also, it can be seen from (a) to (f) that the range of this variation decreases with the increase in the frequency. The peaks of the curves are related to matching cases ($\theta = \theta_{\text{critical}}$).

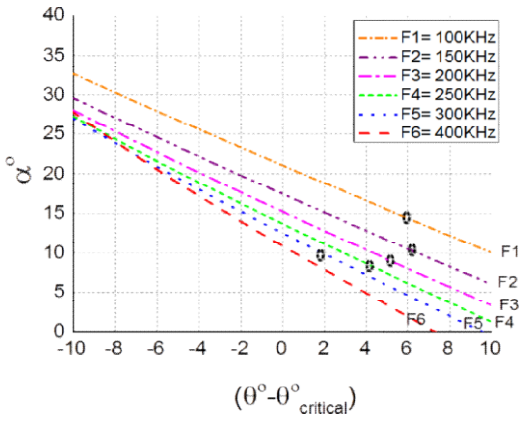

Figure 4. The beaming angles via variation of the incident wave normal angles around the critical angle for different frequencies. Where $\theta = \theta_{\text{critical}}$, the beaming angle is consistent with the conventional LMCT, but for $\theta \neq \theta_{\text{critical}}$, the beaming angle can be larger or smaller than the angle estimated by the Jones' formula. The black circles show the beaming angles observed with multiple satellites with the source at 3.9 Re.

By considering Figure 2 and Figure 4, we can see that for the 100 kHz and 300 kHz frequencies, for example, to have significant efficiency, the scale length should be less than about 100 km and 200 km, respectively.

In Figure 5, we presented the variation of the power transmission function with respect to the wave normal angles around the critical angle (including the critical wave normal angle) for different values of the spatial scale lengths (L). Results presented are for the frequencies of 100 kHz in Figure 5a and 300 kHz in Figure 5b. For f = 100 kHz, from the black circles of Figure 4, $(\theta - \theta_{\text{critical}})$ should be 6° (shown by × mark) and the arrow line shows that the power transmission greater than zero requires L<100 km. For f = 300 kHz, from the black circles of Figure 4, $(\theta - \theta_{\text{critical}})$ should be 2° and the arrow line shows that for greater than zero power transmission, one requires L<200 km.

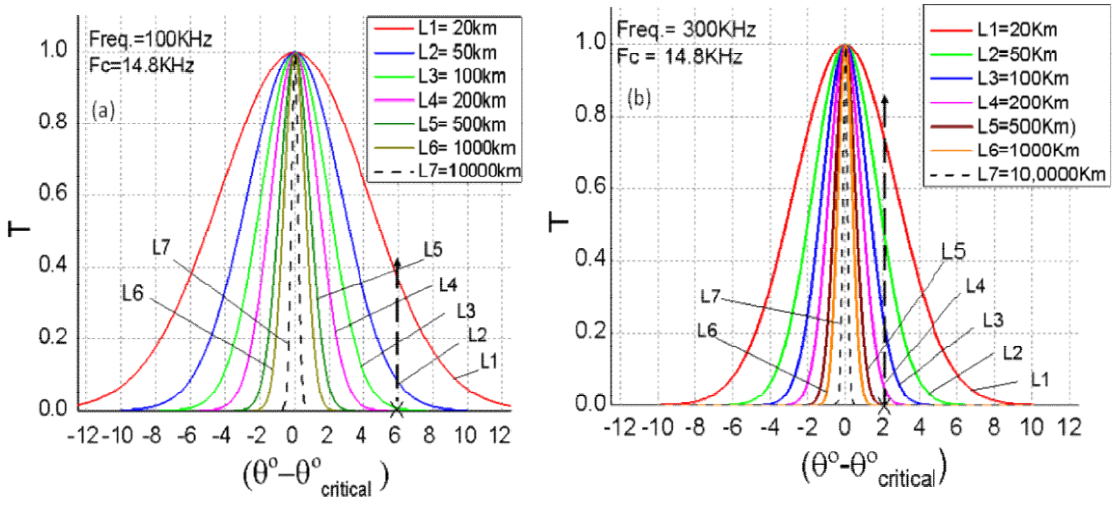

Figure 5. The power transmission function variation with the wave normal angles around the critical angle (including the critical wave normal angle) with different values of the spatial scale lengths (L) for a) f = 100 kHz: according to the black circles of Figure 4 for a case with frequency of 100 kHz, $\theta - \theta_{\text{critical}}$ should be 6° (shown by × mark), the arrow broken line shows that for the power transmission to be greater than zero, L<100 km is needed; and (b) f = 300 kHz: according to the black circles of Figure4 for this case, $\theta - \theta_{\text{critical}}$ should be 2° (shown by × mark) and the arrow broken line shows that for the power transmission to be greater than zero, L<200 km is needed.

4 Conclusions

Since there is a region of evanescence between the two mode branches (ordinary and extraordinary), when the two mode branches are mismatched, the mode conversion efficiency is strongly dependent on the geometrical size of this evanescent region (Kalaee and Katoh, 2014b). A considerable fraction of the energy flux can be transmitted through this region if L becomes small. On the other hand, recent satellite observations have indicated the beaming angle theory is not always consistent with these observations. Also, from recent satellite observations, such as the Cluster mission, structures are found over a broad range of spatial scales with a minimum size of about 20 km.

In this study, we purposed the magnetic field direction perpendicular to the density gradient with a scale length from 20 to 10,000 km, and a range of the frequency from 100 to 400 kHz according to observations of the kilometric continuum (Hashimoto et al., 2006). We calculated the transmitted energy flux via the spatial scale lengths and the frequencies. Also, we calculated the beaming angle versus the frequency. Our results showed that only for a limited range of the wave normal angle variation around the critical angle, there is significant transition energy; with decreasing L, this range becomes larger. Also, with the increase in the frequency, this limitation increases, and there is a narrow range of the wave normal angle variation for the significant transition energy.

Further, the results showed that far away from the critical angle, the variation of the beaming angle is increasing and the beaming angle can be different from the LMCT prediction. Therefore, under the condition that efficient mode conversion is expected due to the effect of the steep density gradient (small L), the radio window angle of the ordinary mode waves could be different from the LMCT prediction, as recently pointed out by the observational results. For these cases, the size of L determines the efficiency of mode conversion. Another possibility for the variation of the beaming angle was considered by Kalaee and Katoh (2014b, 2016), where the external magnetic field vector is not exactly perpendicular to the density gradient vector. They showed that this effect also makes the beaming angle different from the prediction of the beaming theory.

Hence, two effects can change the beaming angle: 1) the existence of an evanescence layer between the two mode branches. For this case, the (mismatch) mode conversion is expected due to the effect of the steep density gradient, and the size of L determines the efficiency of mode conversion; 2) fluctuations in the gradient density that change in the angle between the external magnetic field vector and the density gradient vector can lead to the matching case. Both of the two factors are important and can be applied to the equatorial region of the plasmapause in the Earth's inner magnetosphere, though the second effect seems to be more possible.

References

Boardsen, S. A., Green, J. L., and Reinisch, B. W., 2008, Comparison of kilometric continuum latitudinal radiation patterns with linear mode conversion theory: J. Geophys. Res., **113**, A01219. http://dx.doi.org/10.1029/2007JA012319.

Budden, K. G., 1980, The theory of the radio window in the ionosphere and magnetosphere: J. Atm. Terr. Phys., **42**, 287.

Budden, K. G., 1985, The propagation of the radio waves: Cambridge University Press.

Darrouzet, F., Decreau, P. M. E., De Keyser, J., Masson, A., Gallagher, D. L., Santolik, O., Sandel, B. R., Trotignon, J. G., Rauch, J. L., Le Guirriec, E., Canu, P., Sedgemore, F., Andre, M., and Lemaire, J. F., 2004, Density structures inside the plasmasphere: Cluster observations: Ann. Geophys., **22**, 2577–2585.

Darrouzet, F., De Keyser, J., Décréau, P. M. E., Lemaire, J. F., and Dunlop, M. W., 2006, Spatial gradients in the plasmasphere from Cluster: Geophys. Res. Lett., **33**, L08105, doi: 10.1029/2006GL025727.

Ellis, G. R., 1956, The Z propagation hole in the ionosphere: J. Atm. Terr. Phys., **8**, 43.

Hashimoto, K., Green, J. L., Anderson, R. R., and Matsumoto, H., 2006, In: LaBelle, J. W., and Treumann, R. A., (Eds.), Review of Kilometric Continuum: in Lecture Notes in Physics, **687**, Springer, New York, pp. 37–54.

Jones, D., 1980, Latitudinal beaming of planetary radio emissions: Nature, **288**, 225–229.

Jones, D., 1981, Beaming of terrestrial myriametric radiation: Adv. Space Res., **1**, 373–376.

Jones, D., 1988, Planetary radio emissions from low magnetic latitudes observations and theories: Planetary radio emissions II, edited by Rucker, H. O., Bauer, S. J., and Pedersen, B. M., Austrian Acad. of Sci., Vienna, Austria, **255**.

Jones, D., Calvert, W., Gurnett, D. A., and Huff, R. L., 1987, Observed beaming of terrestrial myriametric radiation: Nature, **328**, 391–395.

Kalaee, M. J., and Katoh, Y., 2014a, A simulation study on the mode conversion process from slow Z-mode to LO mode by the tunneling effect and variations of beaming angle: Adv. Space Res., **54**, 2218–2223.

Kalaee, M. J., and Katoh, Y., 2014b, Effects of the angle between the density gradient and the external magnetic field on the linear mode conversion and resultant beaming angle of LO-mode radio emissions: Earth Moon and Planets, **114**, 1–15.

Kalaee, M. J., and Katoh, Y., 2016, The role of deviation of magnetic field direction on the beaming angle: Extending of beaming angle theory: Atmospheric and Solar Terrestrial Phys., **142**, 35–42.

Kalaee, M. J., Katoh, Y., Kumamoto, A., and Ono, T., 2010, Simulation of mode conversion from upper-hybrid waves to LO-mode waves in the vicinity of the Plasmapause: Ann. Geophys., **28**, 1289–1297.

Kalaee, M. J., Ono, T., Katoh, Y., Iizima, M., and Nishimura, Y., 2009, Simulation of mode conversion from UHR-mode wave to LO-mode wave in an inhomogeneous plasma with different wave normal angles: Earth Planets and Space, **61**, 1243–1254.

Mjulhus, E., 1984, Coupling to Z mode near critical angle: J. Plasma Phys., **31**, 7–28.

Oya, H., 1971, Conversion of electrostatic plasma waves into electromagnetic waves: Numerical calculation of the dispersion relation for all wavelengths: Radio Sci., **12**, 1131–1141.

Oya, H., 1974, Origin of Jovian decametric wave emissions — Conversion from the electron cyclotron plasma wave to the O-mode electromagnetic wave: Planet Space Sci., **22**, 687–708.

Stix, T. H., 1992, Waves in Plasmas: American Institute of Physics, New York.

Warren, E. S., and Hagg, E. L., 1968, Observation of electrostatic resonances of the ionospheric plasma: Nature, **220**, 466–468.